





Original Article

Qingfei Paidu Decoction Inhibits LPS-induced Acute Lung Injury by Targeting the Complement Pathway



Dandan Shi^{1#}, Luna Ge^{1,2#}, Lei Yan³, Yuang Zhang^{1,2}, Ting Wang¹, Yun Geng⁴, Huancai Fan¹, Ruoqia Zhang¹, Zhurui Shao¹, Longjie Hu¹, Jianli Zhao⁵, Shufeng Li⁵, Yi Li⁶, Haojun Shi⁷, Jihong Pan^{1,2}, Guanhua Song^{8*} 
and Lin Wang^{1,2*} 

¹Biomedical Sciences College & Shandong Medicinal Biotechnology Centre, Shandong First Medical University & Shandong Academy of Medical Sciences; NHC Key Laboratory of Biotechnology Drugs, Shandong Academy of Medical Sciences; Key Lab for Rare & Uncommon Diseases of Shandong Province, Shandong, China; ²Department of Rheumatology and Autoimmunology, The First Affiliated Hospital of Shandong First Medical University, Shandong, China; ³Department of Internal Medicine Oncology, Shandong Cancer Hospital and Institute, Shandong First Medical University and Shandong Academy of Medical Sciences, Shandong, China; ⁴Shandong First Medical University & Shandong Academy of Medical Sciences, Shandong, China; ⁵Department of Orthopedic Surgery, The First Affiliated Hospital of Shandong First Medical University, Shandong, China; ⁶Department of Orthopedic Surgery, Shandong Provincial Hospital Affiliated to Shandong First Medical University (Shandong Provincial Hospital), Shandong, China; ⁷The Second Clinical Medical College, Henan University of Chinese Medicine, Zhengzhou, China; ⁸Institute of Basic Medicine, Shandong First Medical University & Shandong Academy of Medical Sciences, Shandong, China

Received: December 17, 2022 | Revised: January 03, 2023 | Accepted: March 19, 2023 | Published online: May 11, 2023

Abstract

Background and objectives: Qingfei Paidu decoction (QFPD) is a compounded Chinese herbal medicine used to treat mild and severe cases of COVID-19. Acute lung injury (ALI) is a common clinical manifestation of COVID-19, and this mainly manifests through lung inflammation and epithelial cell damage. However, the mechanism by which QFPD ameliorates ALI remains unclear. The present study aims to determine the role and molecular mechanism of QFPD in lipopolysaccharide (LPS)-induced ALI in mice.

Keywords: Traditional Chinese medicine; Acute lung injury; Complement pathway; Network pharmacology.

Abbreviations: ALI, acute lung injury; ARDS, acute respiratory distress syndrome; ANOVA, one-way analysis of variance; BALF, bronchoalveolar lavage fluid; BP, biological process; CC, cellular component; CCK-8, cell counting Kit-8; CSS, cytokine storm syndrome; CXCL2, C-X-C Motif Chemokine Ligand 2; COVID-19, 2019 novel coronavirus disease; DAPI, 4',6-diamidino-2-phenylindole; DEGs, differentially expressed genes; ELISA, enzyme-linked immunosorbent assay; GO, Gene Ontology; H&E, hematoxylin and eosin; IF, immunofluorescence; IFN- γ , interferon-gamma; IL1 β , interleukin 1 beta; IL6, Interleukin-6; KEGG, Kyoto Encyclopaedia of Genes and Genomes; LPS, lipopolysaccharide; MCP-1, monocyte chemoattractant protein-1; MF, molecular function; NO, nitric oxide; OB, bioavailability; PBS, phosphate buffered saline; PPI, protein-protein interaction networks; QFPD, Qingfei Paidu decoction; qRT-PCR, quantitative real-time PCR; RT, room temperature; SARS-COV-2, severe acute respiratory syndrome coronavirus 2; siRNA, small interfering RNA; TCM, traditional Chinese medicine; TC-MSP, traditional Chinese medicine systems pharmacology; TNF- α , tumor necrosis factor-alpha; TUNEL, TdT-mediated dUTP nick-end labeling; W/D, lung wet/dry; VEGF- β , vascular endothelial growth factor- β .

*Correspondence to: Guanhua Song, Institute of Basic Medicine, Shandong First Medical University & Shandong Academy of Medical Sciences, No. 6699, Qingdao Road, Jinan, Shandong 250117, China. ORCID: <https://orcid.org/0000-0002-1359-515X>. Tel: +860531-59567360, Fax: +860531-59556660, E-mail: yysghyy@163.com; Lin Wang, Biomedical Sciences College & Shandong Medicinal Biotechnology Centre, Shandong First Medical University & Shandong Academy of Medical Sciences, No. 6699, Qingdao Road, Jinan, Shandong 250117, China. ORCID: <https://orcid.org/0000-0002-5478-0212>. Tel: +860531-59567360, Fax: +860531-59556660, E-mail: linwang@sdfmu.edu.cn

#These authors contributed equally to this work.

How to cite this article: Shi D, Ge L, Yan L, Zhang Y, Wang T, Geng Y, et al. Qingfei Paidu Decoction Inhibits LPS-induced Acute Lung Injury by Targeting the Complement Pathway. *Explor Res Hypothesis Med* 2023;8(3):215–228. doi: 10.14218/ERHM.2022.00127.

Methods: After the administration of QFPD treatment in LPS-induced ALI mice, the therapeutic effect was evaluated through the H&E staining of lung tissues and the level of inflammatory factors *in vivo*. The RNA sequencing in mouse peritoneal macrophages and subsequent network pharmacological analysis were used to explore the molecular mechanisms of QFPD. Experimental validation was also performed by immunofluorescence staining, enzyme-linked immunosorbent assay (ELISA), and western blot.

Results: QFPD inhibited the LPS-induced inflammatory cytokines in macrophages, ameliorated ALI in mice, and prolonged its survival at the lethal dose of LPS. Furthermore, the complement-related pathway was enriched through the network pharmacology and transcriptome analysis of the gene expression. The quantitative real-time PCR and apoptotic analysis further confirmed that QFPD inhibited ALI through the classical complement pathway as no additive changes were observed when its key components were silenced plus QFPD treatment.

Conclusions: QFPD applied for the treatment of COVID-19 can attenuate ALI through the classical complement pathway. The present study provides a practical basis and directional guide for the further exploration of the use of QFPD in treating ALI.

Introduction

The main features of acute lung injury (ALI) are acute, progressive respiratory failure and hypoxemia, which are typical clinical manifestations of thoracic diseases.¹⁻³ During the outbreak of the 2019 novel coronavirus disease (COVID-19), SARS-CoV-2 infection induced the excessive activation of immune cells in the body's lungs,^{4,5} and this led to the development of ALI.

The response of ALI to severe pulmonary microbial infections is the result of the immune recognition of pathogens responsible for the induction of pro-inflammatory immune responses.⁶ ALI leads to severe tissue damage, and in severe cases, irreversible lung damage, leading to death.^{7,8} Macrophages are the most abundant immune cells in healthy lungs, and are essential for maintaining lung homeostasis.^{9,10} Macrophage dysregulation in the lungs is the major cause of inflammation in bacterial and viral infections, and a key factor in the pathogenesis of ALI and acute respiratory distress syndrome, including the involvement of cytokine storms.¹¹ For example, macrophages in Gram-negative bacterial pneumonia produce tumor necrosis factor- α (TNF- α), which induces granulocyte-macrophage colony-stimulating factor in alveolar epithelial cells, and proliferative signals through autocrine stimulation, thereby contributing to the impaired recovery of alveolar epithelial cells.¹²

Qingfei Paidu decoction (QFPD) was created by Ge You-wen, a distinguished researcher of the Chinese Scientists of Traditional Chinese Medicine, based on the core pathogenesis of COVID-19, combined with classic prescriptions in the "Treatise on Febrile and Miscellaneous Diseases", which include the Maxing Shigan Decoction, Shegan Mahuang Decoction, Xiaochaihu Decoction, and Wuling Powder.¹³ This was listed in the Chinese Pharmacopoeia (2015 Edition), and is helpful for the prevention and treatment of influenza H1N1 and hand-foot-and-mouth disease.¹⁴ Furthermore, QFPD is useful for treating COVID-19, and is recommended for SARS-CoV-2 infection.¹⁵ The complement signaling pathway can be activated in three different ways: classical pathway, lectin pathway, and alternative pathway.¹⁶ This plays an important role in systemic inflammatory response.¹⁷⁻¹⁹ After binding to its receptor, this can activate its effector, and induce the production of inflammatory cytokines.^{18,20} The present study determined the role of QFPD in lipopolysaccharide (LPS)-induced ALI through a suite of cell experiments and animal experiments. This will provide a practical basis and directional guide for the further exploration of the use of QFPD for treating ALI.

Materials and methods

QFPD components and preparation of the drug-containing serum

QFPD comprises of 21 traditional Chinese herbs: Ephedra 9 g, Radix glycyrrhizae 6 g, Almonds 9 g, raw gypsum 15g, Ramulus Cinnamomi 9 g, Rhizoma alismatis 9 g, Polyporus umbellatus 9 g, Atractylodes japonica Koidzumi 9 g, Poria 15 g, Bupleurum 16 g, Scutellaria 6 g, Ginger-processed Pinellia 9 g, Ginger 9 g, Radix et Rhizoma Asteris 9 g, Flos Farfarae 9 g, Rhizoma Belamcandae 9 g, Radix et Rhizoma Asari 6 g, Rhizoma Dioscoreae 12 g, Fructus Aurantii Immaturus 6 g, Pericarpium Citri Reticulatae 6 g, and Herba Agastachis 9 g. Gypsum was initially decocted with 250 mL of water for 30 minutes. Then, the remaining herbs were mixed with 500 mL of water, and steeped for 30 minutes. The water decoction was prepared according to the traditional method. In the present study, the doses administered to mice were converted based on human clinical doses.

All animal studies were approved by the Institutional Animal Care and Use Committee of Shandong First Medical University & Shandong Academy of Medical Sciences (SMBC21LL028). Mice (Wistar, male, 280 g; Pengyue, Jinan, China) were gavaged with QFPD (3.6 mL) or saline for six consecutive days. At one hour after the last gavage, the mice in each group were anesthetized with 2% pentobarbital sodium (0.2 mL/100 g). Then, blood was drawn from the abdominal aorta, held at 37°C for one hour, and centrifuged at 2,000 rpm for five minutes to collect the serum. Afterwards, the serum was inactivated at 56°C, filtered, and stored at -20°C for back-up.

High performance liquid chromatography

Initially, appropriate amounts of chlorogenic acid, amygdalin, geniposide, hesperidin, baicalin, liquiritin and ammonium glycyrrhetate reference substance were taken, and the mixed reference substance solution was prepared by adding the methanol solution. Then, 5 mL of QFPD was extracted by ultrasonic extraction with 4 mL of methanol, and centrifuged at 2,000 rpm for 10 minutes. Afterwards, the supernatant was taken and filtered through a 0.22 μ m filter membrane to obtain the QFPD sample solution. The above-mentioned mixed reference solution and QFPD test solution were determined by high performance liquid chromatography. The chromatographic conditions were, as follows: 0.1% phosphoric acid water and acetonitrile as the mobile phase, 210 nm detection wavelength, column temperature at 25°C, flow rate at 0.8 mL/min, and injection volume of 5 μ L.

Cell culture, isolation and stimulation

The peritoneal macrophages were isolated and cultured, as previously described.²¹ Briefly, eight-week-old male C57 mice (Pengyue, Jinan, China) were intraperitoneally (i.p.) injected with 1 mL of 3% mercaptoacetic acid salt once a day for three consecutive days, and the peritoneal macrophages were obtained from these mice. Then, 5 mL of pre-cooled phosphate buffered saline (PBS) was injected into the peritoneal cavity, and the peritoneal lavage solution was repeatedly rinsed twice. Afterwards, the lavage solution was centrifuged at 1,000 r/min for 10 minutes in room temperature, and the resulting cell precipitates were re-inoculated with 10% RPMI 1640 culture solution. Subsequently, the macrophages were purified using RPMI 1640 (Gibco Life Technologies), and lavaged twice with PBS (Solarbio, Beijing, China) after four hours of adherence. The remaining adherent cells were macrophages, and these were cultivated in RPMI at 37°C and 5% CO₂. Before treatment with the QFPD-containing serum or siRNA, the peritoneal macrophages were cultured in DMEM, which contained 2% fetal bovine serum, overnight. Then, these were stimulated with LPS (1 μ g/mL; Sigma-Aldrich, St. Louis, MO, USA), and used to induce cell inflammation.

Cell viability assay

Cell viability was measured using Cell Counting Kit-8 (CCK-8; Solarbio, Beijing, China). Briefly, macrophages were seeded in a 96-well plate, and allowed to adhere overnight. Then, the cells were treated with LPS, with or without QFPD, for 24 hours. Afterwards, 10 μ L of CCK-8 solution was added and incubated at 37°C for one hour. Subsequently, a microplate reader (SpectraMax ID3, Shanghai, China) was used to measure the absorbance at a wavelength of 450 nm.

Nitric oxide (NO) detection

Macrophages were seeded in a 6-well plate, and allowed to adhere

Table 1. All primers used for the study

Gene names	Primer sequence (5'-3')	GeneBank accession no.	Product size (bp)
MCP-1	TAAAAACCTGGATCGGAACCAAA	NM_011333	120
IFN- γ	ATGAACGCTACACACTGCATC	NM_008337	182
VEGF- β	CTTCAATACGTCAGACATTCGGG	NM_011577	142
CXCL2	CCAACCACCGCTACAGG	NM_002089.4	108
TNF- α	CCTGTAGCCCACGTCGTAG	NM_013693	148
IL-1 β	GAAATGCCACCTTTTGACAGTG	NM_008361	116
MMP3	TCTGGGCTATACGAGGGCAC	NM_010809	232
MMP9	GCAGAGGCATACTTGACCG	NM_013599	229
GAPDH	AGGTCGGTGTGAACGGATTG	NM_008084	95

CXCL2, C-X-C Motif Chemokine Ligand 2; GAPDH, Glyceraldehyde-3-Phosphate Dehydrogenase; IFN- γ , interferon-gamma; IL-1 β , interleukin 1 beta; MCP-1, monocyte chemoattractant protein-1; MMP, matrix metalloproteinase; TNF- α , tumor necrosis factor-alpha; VEGF- β , vascular endothelial growth factor- β .

overnight. Then, after cells were administered with LPS, with or without QFPD, for 24 hours, the culture supernatants were collected and centrifuged at 1,000 g for three minutes to remove the floating cells. Afterwards, the NO level of the culture supernatants was detected using a NO detection kit (Beyotime Biotechnology, Shanghai, China), and the absorbance was measured at 550 nm using a microplate reader.

Animals and treatment

ALI was established through a single i.p. injection of LPS (15 mg/kg). After four hours, a subset of mice was sacrificed for serum collection. At eight hours after induction, the other part of each of the mouse's left bronchus was ligated and perfused with saline (1 mL) into the right lung lobe to obtain the bronchoalveolar lavage fluid (BALF). The serum and BALF collected above were subjected to multi-cytokine analysis, and the left lung was fixed with paraformaldehyde for histological analysis. In order to analyze the effect of QFPD on the survival time of cytokine storm syndrome (CSS) model mice, the i.g. injection of saline ($n = 10$) or QFPD (0.8 mL) was performed before the i.p. injection of the lethal dose of LPS (30 mg/kg) to mice. Mice survival was recorded every two hours, up to 40 hours. All animal studies were approved by the Institutional Animal Care and Use Committee of Shandong First Medical University & Shandong Academy of Medical Sciences (SMBC21LL028).

Lung wet/dry (W/D) ratio

The W/D weight ratio was determined to measure the lung tissue edema. Briefly, the whole lung was harvested, the surface water was allowed to dry, and the wet weight was measured. Then, the baseline dry weight of the lung was calculated by heating the lung tissue in a thermostatic oven at 80°C for 48 hours.

Quantitative real-time polymerase chain reaction (qRT-PCR) and enzyme-linked immunosorbent assay (ELISA)

The total RNA was isolated from cultured cells using TRIzol reagent (Vazyme, Nanjing, Jiangsu, China) for reverse transcription using the ReverTra Ace qPCR RT Kit (TOYOBO, Shanghai, China). Then, qRT-PCR was carried out using the Light-Cycler 480 (Roche, Basel, Switzerland), and the primers created through BGI (Beijing, China). The primer sequences are listed in Table 1. The secreted levels of C3a, C5a and C5b-9 (Elabscience, Wuhan, Hubei, China), and inflammatory cytokines in the culture super-

natants and serum were measured using ELISA kits (Hangzhou Multi-Science Company, Hangzhou, Zhejiang, China).

Small interfering RNA (siRNA) transfection and RNA sequencing

Small interfering RNA (siRNA, Table S1) against C3, C1s, CFD and MASP2, and the negative control (Ruibo, Guangzhou, China) were transfected to the macrophages using transfection reagents (Polyplus-transfection, Strasbourg, France). For the RNA sequencing, the LPS-activated macrophages were treated with QFPD for 24 hours. Then, the total RNA was collected to construct the cDNA library for the RNA transcriptome sequencing through LC-BIO Technologies Co., Ltd. (Hangzhou, Zhejiang, China).

Western blot

After LPS-activated macrophages were treated with QFPD-mediated serum for 24 hours, these macrophages were washed with PBS for three times, and the protein components were extracted using radioimmunoprecipitation assay lysate and phenylmethane-sulfonyl fluoride (100:1). The protein concentration was detected using the Bradford Protein Assay Kit (Beyotime Biotechnology, Shanghai, China). The primary antibodies against BAX (50599-2-Ig, 1:5,000), Bcl2 (26593-1-AP, 1:2,000), GAPDH (60004-1-Ig, 1:5,000), and caspase-3 (19677-1-AP, 1:1,000) were purchased from Proteintech (Wuhan, Hubei, China). The cleaved-caspase-9 (#7237P, 1:1,000), cleaved-caspase-7 (#8438P, 1:1,000), and BAK (#6947P, 1:1,000) were purchased from Cell Signaling (Danfoss Town, Boston, Massachusetts, USA). Sodium dodecyl-sulfate polyacrylamide gel electrophoresis (SDS-PAGE) was performed to separate the samples, and these were transferred onto polyvinylidene difluoride membranes for visualization using the ECL Plus detection system (Thermo Scientific, Waltham, MA, USA).

TdT-mediated dUTP nick-end labeling (TUNEL) staining

The left lung lobes of mice were fixed with 4% paraformaldehyde (Solarbio, Beijing, China). Then, the tissues were embedded in paraffin, sliced, and stained with TUNEL (Solarbio, Beijing, China), according to manufacturer's instructions. Afterwards, these were incubated with 4',6-diamidino-2-phenylindole (DAPI; Beyotime Biotechnology, Shanghai, China) to identify the nucleus. Subsequently, the cells were observed using a laser scanning confocal microscope (Olympus, Japan).

Immunofluorescence (IF)

After the LPS-activated macrophages were treated with QFPD-medicated serum for 24 hours, these were fixed for 15 minutes in room temperature (RT), and treated with the immunochromatin penetrant (Beyotime Biotechnology, Shanghai, China) for 30 minutes in RT. After blocking with the QuickBlacktm Immunochrome blocking solution (Beyotime Biotechnology, Shanghai, China) for one hour, the cells were incubated overnight with the primary antibody at 4°C. On the second day, these cells were allowed to re-warm for one hour at 37°C, incubated with the secondary antibody for one hour, and subsequently incubated with DAPI to identify the nucleus. Then, these cells were observed by laser scanning confocal microscopy.

Histological analysis

The lung lobes were fixed with 4% paraformaldehyde, or the paraffin embedment sections (5 μm) obtained from formalin-fixed tissues were stained with hematoxylin and eosin (H&E; Solarbio, Beijing, China), and were photographed using a microscope (Olympus, Tokyo, Japan).

Tissue immunofluorescence

The mice lung lobes were fixed with 4% paraformaldehyde and paraffin-embedded, and the tissue sections (5 m) were formalin-fixed. Then, the paraffin sections were dewaxed and hydrated, and antigen repair was performed using the sodium citrate-EDTA antigen repair solution (Beyotime Biotechnology, Shanghai, China) for 20 minutes after blocking with 5% BSA (Solarbio, Beijing, China) for one hour. Afterwards, the sections were incubated with the primary antibody overnight at 4°C. On the second day, the sections were allowed to rewarm for one hour at 37°C, cultured with the secondary antibody for one hour at 37°C, and incubated with DAPI to identify the nucleus. The cells were observed by laser scanning confocal microscopy.

Network pharmacology analysis

The active ingredients of the herbs in QFPD were collected from the Traditional Chinese Medicine Systems Pharmacology Database and Analysis Platform (TCMSP, old.tcmsp.com/tcmsp.php).²² The obtained components were filtered, as follows: 180 ≤ molecular weight ≤ 500, dehydration partition coefficient < 5, bioavailability (OB) ≥ 30%, and drug-like property ≥ 0.18.²³⁻²⁶ The targets for each component were predicted using the PharmMapper (lilab-ecust.cn/pharmmapper/)²⁷ and TargetNet database (targetnet.scbdd.com/calcnnet/index/).²⁸ Duplicate targets were removed after merging.

The ALI-related targets were collected using “acute lung injury” as the keyword from the GeneCards database (www.genecards.org/),^{22,28} Online Mendelian Inheritance in Man database (www.omim.org/),²² and Therapeutic Target Database, db.idrblab.net/ttd). The online mapping platform Venny 2.1^{29,30} was used to map the targets of the effective components of QFPD and disease targets of ALI, and a Venn diagram was drawn to indicate the relationship between each target set, with the overlapping region potentially including the key targets for QFPD to treat ALI. Next, the common targets were uploaded into the STRING database,^{30,31} multiple proteins were selected, and Homo sapiens were selected as the species. Then, the interaction between target proteins was analyzed, and a network diagram for the protein-protein interaction (PPI) was obtained. The Cytoscape 3.9.1 software was used for visualization.³²

Gene Ontology (GO) and Kyoto Encyclopedia of Genes and Genomes (KEGG) enrichment analysis

The identified gene targets for QFPD (refer to section 2.15) were copied to the list of the DAVID database (david.ncicrf.gov/tools.JSP),³³ the marker official_gene_symbol was selected, and Homo sapiens were annotated for the GO TERM (biological process [BP], cellular component [CC], and molecular function [MF]), enrichment analysis, and KEGG pathway annotation analysis of target proteins. The key GO and KEGG pathways were identified using $p < 0.05$ as the criterion. Cytoscape 3.9.1 was used to construct the drug-herb-active compound network.

Statistical analysis

The data was presented as mean ± standard deviation. The “*n*” represented the number of independent experiments performed in mouse peritoneal macrophages ($n = 6$) for the cell experiments. Using randomization and blind analysis, all animal experiments were designed to generate groups of equal size ($n = 9$). One-way analysis of variance (ANOVA) was used to compare multiple groups. Statistical significance was set at $p < 0.05$. Analysis and graphing were performed using the GraphPad Prism 8.0 software (San Diego, CA, USA).

Results

Therapeutic effects of QFPD on LPS-induced ALI in mice

The therapeutic impact of QFPD on ALI was assessed using the LPS-induced mouse model. Before the experiment, the fingerprint of the synthesized QFPD was initially established (Fig. S1). Then, QFPD was consecutively administered for three days before LPS injection, and the serum was collected at four hours following LPS injection for further analysis. Twelve cytokines were simultaneously measured by ELISA. Compared to the controls, the production of five cytokines (Interleukin-6 (IL6), interferon-gamma (IFN-γ), chemokine monocyte chemoattractant protein-1 (MCP-1), TNF-α and interleukin 1 beta (IL1β)) significantly decreased after the QFPD treatment (Fig. 1a).

In order to assess the inflammation status in the lungs, ELISA was performed to examine the production of 12 cytokines in BALF at eight hours after LPS stimulation. The secreted levels of six cytokines (IFN-γ, MCP-1, IL6, TNF-α, IL1β and granulocyte-macrophage colony-stimulating factor) significantly decreased after QFPD treatment, when compared to the parental controls (Fig. 1b). The histological analysis revealed alveolar damage in animals that were given LPS (i.p.) injections, which included inflammatory cell infiltration (orange arrow), congestion (blue arrow), and edema within thickened alveoli (black arrow) (Fig. 1c). However, the above pathological parameters were all ameliorated by the QFPD treatment.

Next, the lung injury scores were calculated (Fig. 1d), and the protective effects of QFPD were observed when the score was 2.6 ± 0.61 , when compared to the control group (score: 4.8 ± 0.33). Furthermore, the QFPD treatment prolonged the survival time of mice that received the i.p. injection of the lethal dose of LPS (30 mg/kg), when compared to the controls (Fig. 1e). The lung W/D ratio was used to measure the effects of QFPD in pulmonary edema. As shown in Figure 1f, the lung W/D ratio significantly increased in the LPS-treated group, when compared to the control group, while this increase was reduced by the QFPD treatment. The routine blood test revealed that the exposure to LPS led to the increase in granulocytes and decrease in lymphocytes, when

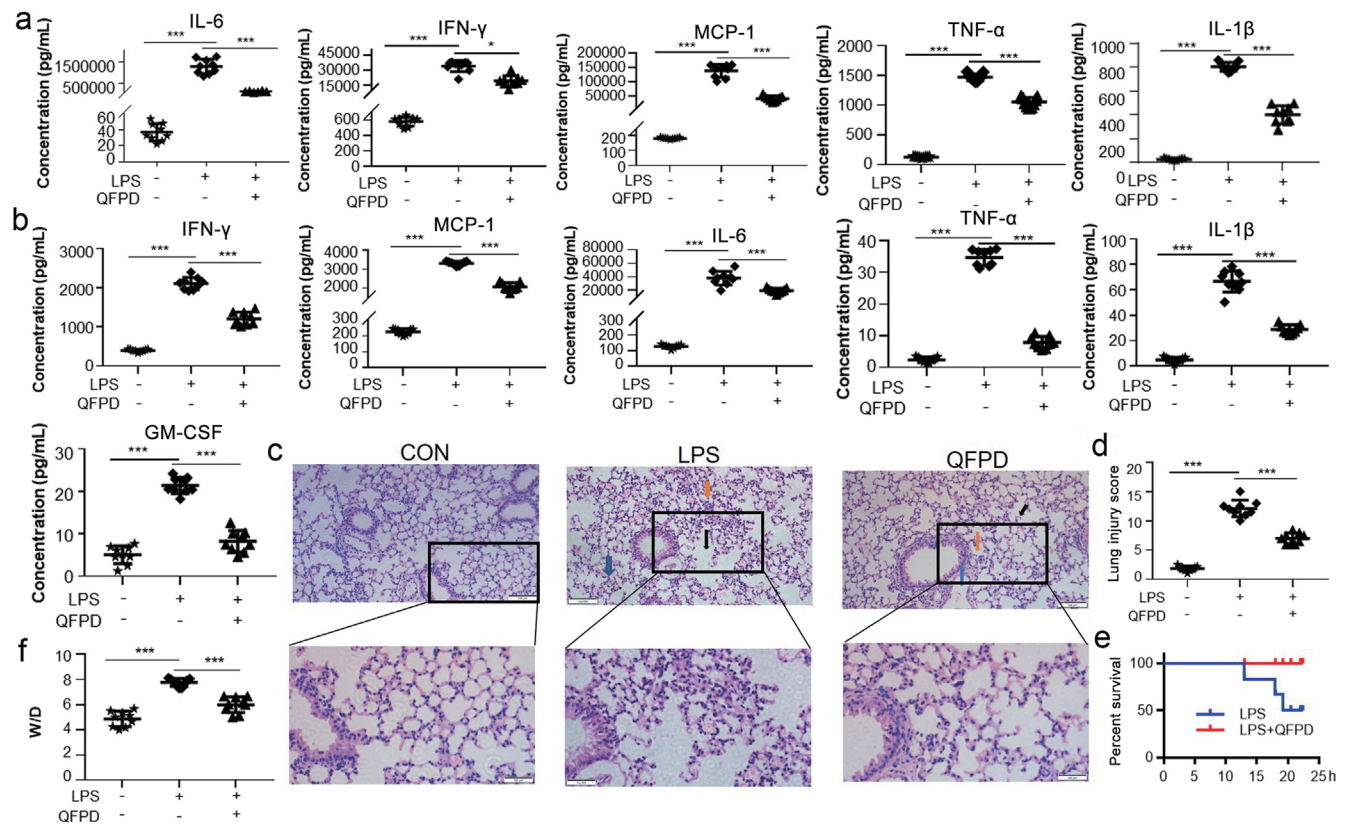


Fig. 1. QFPD exerts protective effects against LPS-induced ALI *in vivo*. (a and b) QFPD reduced the levels of pro-inflammatory cytokines IL6, INF- γ , MCP-1, TNF- α and IL1 β in serum (a) and BALF (b). (c) Representative images of the lung H&E staining for the control, LPS, and LPS+QFPD groups. The black, blue and orange arrows indicate the infiltration of inflammatory cells, congestion, and edema within the thickened alveolar, respectively. Scale bars: 200 μ m, as indicated. (d) Lung injury scores for the control, LPS, and LPS+QFPD treatment groups ($n = 6$). (e) Survival time of LPS-induced CSS mice in the control (LPS, blue line) and QFPD (10% QFPD-medicated serum) (LPS+QFPD, red line) groups ($n = 10$). (f) Lung wet/dry (W/D) ratio. The dissected lung tissues were weighed and oven dried at 80°C for 48 hours to calculate the W/D ratio. (a–f) Statistical analysis was performed using one-way ANOVA, followed by Tukey-Kramer post-test, $^{**}p < 0.01$, $^{***}p < 0.001$, compared to the control group. ANOVA, one-way analysis of variance; BALF, bronchoalveolar lavage fluid; CSS, cytokine storm syndrome; GM-CSF, Granulocyte-macrophage colony-stimulating factor; H&E, hematoxylin and eosin; INF- γ , interferon-gamma; IL1 β , interleukin 1 beta; IL6, Interleukin-6; LPS, lipopolysaccharide; MCP-1, monocyte chemoattractant protein-1; TNF- α , tumor necrosis factor-alpha; QFPD, Qingfei Paidu decoction; W/D, lung wet/dry.

compared to the parental controls. Obviously, after treatment with QFPD, the above changes were all restored (Table S2).

QFPD alleviates the lung injury by inhibiting inflammation and apoptosis

Mouse peritoneal macrophages were used to analyze the anti-inflammatory potential of QFPD. In order to obtain the optimal concentration of QFPD, cell counting was initially performed using the CCK-8 kit. As shown in Figure 2a, low concentrations of drug-containing serum did not have a significant effect on the growth of peritoneal macrophages. When the concentration of drug-containing serum was at 15%, the cell proliferation started to be inhibited. Consequently, 10% QFPD-medicated serum was chosen for the subsequent cellular assay.

As reported by previous studies, LPS (1 μ g/mL) was used to stimulate macrophages to mimic the acute inflammation, and this evidenced by the sharp increase in TNF- α secretion in macrophages (Fig. 2b). However, the increase was mostly reversed after the QFPD treatment. Similar effects were observed by analyzing the production of MCP-1, IFN- γ , vascular endothelial growth factor- β (VEGF- β), IL1 β , matrix metalloproteinase (MMP)-9 and C-X-C Motif Chemokine Ligand 2 (CXCL2). In order to examine the ef-

fect of QFPD on NO production, the cells were pretreated with QFPD for one hour, and subsequently stimulated with LPS (1 μ g/mL) for another 24 hours. Consistently, the increase in NO production caused by the LPS stimulation was attenuated by the QFPD treatment (Fig. 2c).

During an inflammation response, the excessive production of pro-inflammatory cytokines can induce the apoptosis of inflammatory cells (Karki *et al.*, 2021).⁴ In order to determine whether QFPD can modulate the apoptosis of pulmonary cells in LPS-exposed lungs, the expression of apoptosis-associated proteins was detected by IF. As shown in Figure 3a, the LPS-treated group exhibited an increase in caspase-3 and BAX expression, and a decrease in BCL-2 expression, when compared to the control group. In contrast, the QFPD treatment prevented this trend within four hours after LPS exposure. In addition, the inhibition of LPS-induced apoptosis by QFPD was identified by TUNEL assay (Fig. 3b). Furthermore, the induction of apoptosis through the challenge of LPS was confirmed by western blot analysis, showing the increase in Bax, caspase-3 and cleaved caspase-9, and the decrease in Bcl-2 in lung tissues (Fig. 3c) and macrophages (Fig. 3d). As expected, the above parameters were all restored after QFPD treatment, suggesting the protective role of QFPD against the LPS-

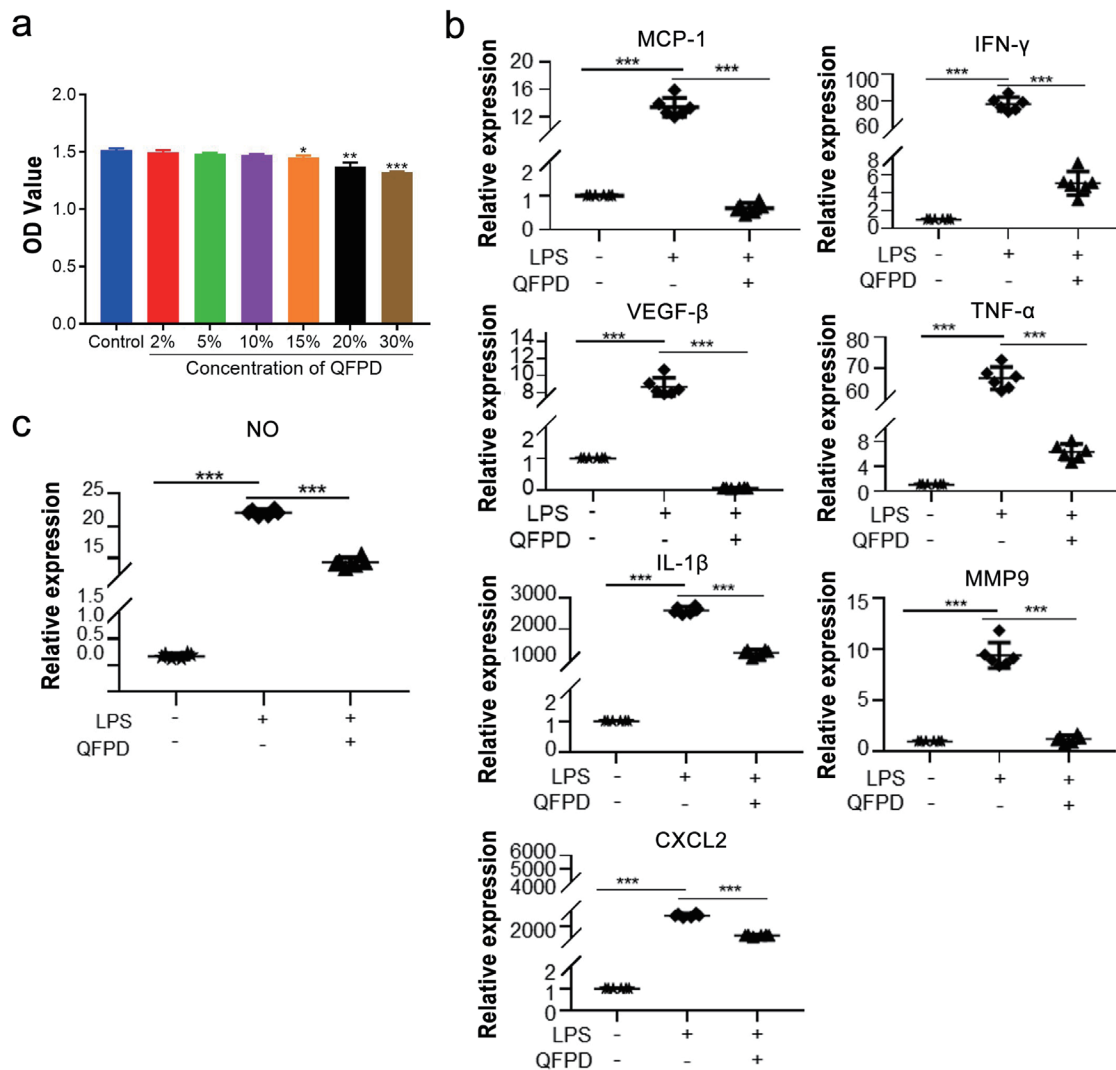


Fig. 2. QFPD inhibits the inflammatory response in LPS-induced macrophages *in vitro*. (a) Cell viability assay for the mouse peritoneal macrophages. (b) QFPD inhibited the expression of MCP-1, INF- γ , VEGF- β , TNF- α , IL1 β , MMP-9 and CXCL2 *in vitro*. (c) QFPD inhibited the nitric oxide production. Statistical analysis was performed using one-way ANOVA, followed by Tukey-Kramer post-test, ** $p < 0.01$, *** $p < 0.001$, compared to the control group. ANOVA, one-way analysis of variance; CXCL2, C-X-C Motif Chemokine Ligand 2; INF- γ , interferon-gamma; IL1 β , interleukin 1 beta; LPS, lipopolysaccharide; MCP-1, monocyte chemoattractant protein-1; MMP-9, matrix metalloproteinase 9; QFPD, Qingfei Paidu decoction; VEGF- β , vascular endothelial growth factor- β .

induced apoptosis of pulmonary tissue cells.

QFPD treatment induces an altered molecular signature in immune cells

In order to determine the possible mechanisms underlying the therapeutic effects of QFPD in ALI, transcriptome sequencing (RNA-seq) analysis was performed to identify the differentially expressed genes (DEGs) in LPS-activated macrophages versus LPS-activated macrophages plus QFPD treatment.

A total of 182 genes were identified to be significantly differentially expressed (Fig. 4a), and the enrichment analysis of the GO classification and KEGG pathways was conducted to identify the associated biological processes. The DEGs were enriched in the complement component C5a signaling pathway, complement component C5a receptor activity, inflammatory response, positive regulation of cytosolic calcium ion concentration, cellular

response to lipopolysaccharide, and regulation of IL8 production (Fig. 4b and d). The KEGG analysis revealed that the DEGs were mainly involved in nitrogen metabolism, cysteine, and methionine metabolism, the complement and coagulation cascades, and the IL17 signaling pathway (Fig. 4c).

Pharmacological analysis results for the QFPD Network

A total of 819 genes related to ALI were collected from the GeneCards, Therapeutic Target Database, and Online Mendelian Inheritance in Man data collection databases. By employing three available resources, namely, the PharmMapper, TargetNet, and SwissTargetPrediction databases, a total of 362 unique targets were finally collected. Then, the above potential target genes of QFPD were intersected with the targets of ALI, and it was identified that 52 genes may be associated with the effects of the QFPD treatment in ALI (Fig. 5a). Subsequently, these 52 overlapping tar-

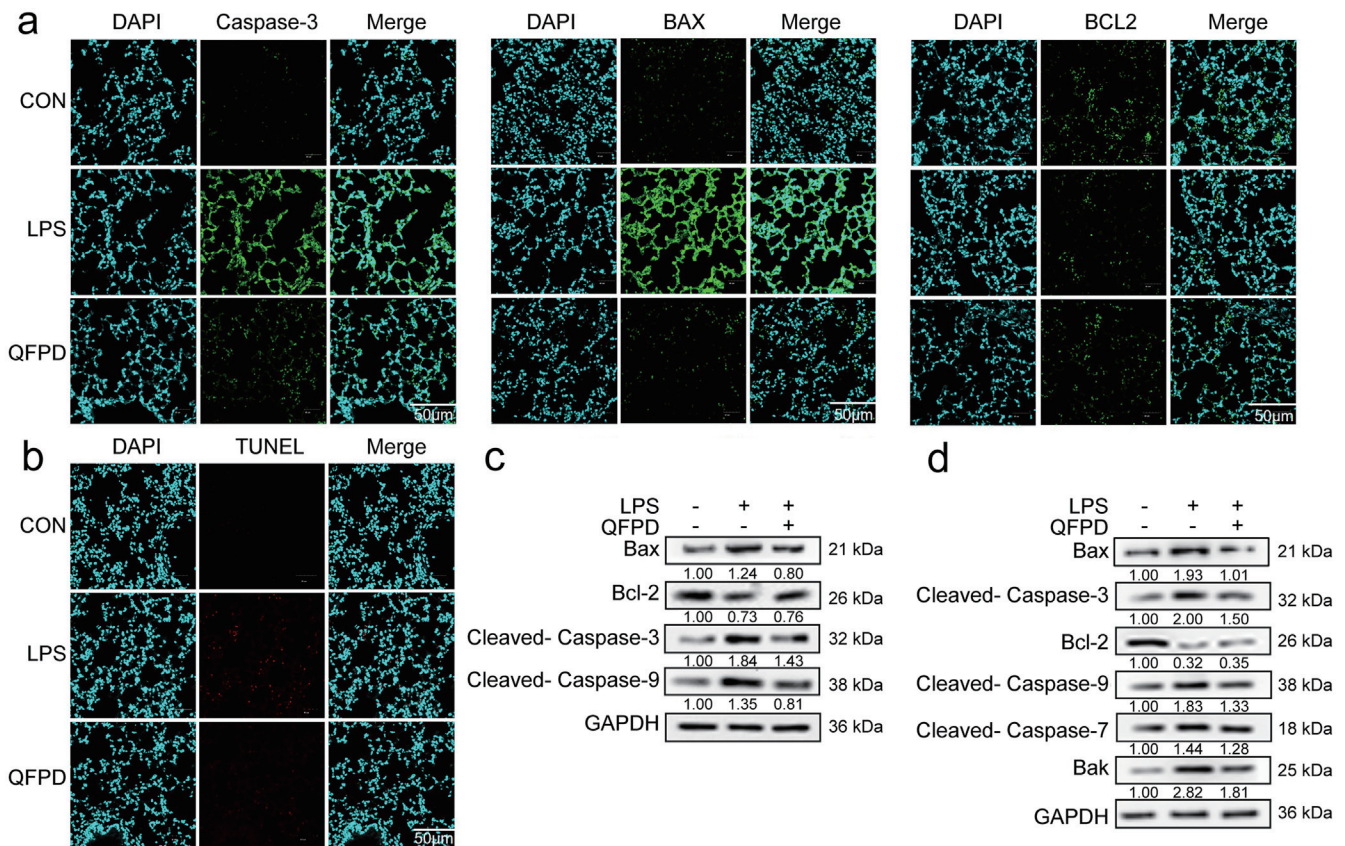


Fig. 3. Effects of QFPD on apoptosis. (a) Tissue immunofluorescence staining of the caspase-3, Bax, and Bcl-2 protein (magnification: 400×). (b) TUNEL staining. (c) Effect of QFPD on the protein expression of Bax, Bcl-2, caspase-3, and cleaved-caspase-9. The protein expression was measured through the western blot analysis of lung tissues. (d) Effect of QFPD on the protein expression of Bax, caspase-3, Bcl-2, cleaved-caspase-9, cleaved-caspase-7, and Bak. The protein expression was measured through the western blot analysis of peritoneal macrophages. LPS, lipopolysaccharide; QFPD, Qingfei Paidu decoction.

gets were imported into the STRING database to build the PPI network (Fig. 5b), and visualized using Cytoscape. Using this network, 10 core targets were obtained: TNF, EGFR, NR3C1, AR, NOS3, MAPK14, GRIN2B, RELA, MMP9 and HTR2A (Fig. 5c). The molecular docking of core targets was also performed (Fig. S2). These targets may be regarded as the primary action targets of QFPD for the therapy of ALI. The discovery of these targets demonstrates that QFPD treats ALI through a variety of potential targets.

The names of the active ingredients of QFPD (Table S3) were imported into the Cytoscape software to build a drug-ingredients network diagram (Fig. 5d). In addition, the compounds and associated targets from the QFPD formula were imported to Cytoscape to create a compound-target network map (Fig. 6a). The Cytoscape software Network Analyzer plug-in was used to generate and assess the network's topological parameters from the standpoint of network node relevance. Then, degree was selected as a measurement of node importance, in which degree referred to the number of edges associated with a node. Thus, a larger node meant more importance. According to the degree analysis, the top six compounds were, as follows: MOL005918 (phenanthrene), MOL000822 (polyporusterene G), MOL006129 (6-methylgingediacetate2), MOL004948 (isoglycyrol), MOL005890 (pachypodol), and MOL001689 (acacetin).

The R programming language and DAVID database were used

for the GO enrichment analysis of the above-mentioned QFPD targets to treat COVID-19. The top 20 enriched categories, which include BP, CC and MF, are listed in Figure 6b. For BP, the target genes were involved in the following areas: regulation of cytokine production, apoptotic signaling pathway, angiogenesis, vasculature development, and response to xenobiotic stimulus. For CC, the targets were enriched in the membrane raft, membrane microdomain, postsynaptic membrane, and others. For MF, the target genes were extensively involved in the following areas: amine binding, serotonin binding, nuclear receptor activity, ligand-activated transcription factor activity, transcription coactivator binding, and nuclear receptor activity. The KEGG result included 53 pathways (Fig. 6c), such as the AGE-RAGE signaling pathway in diabetic complications, alcoholic liver disease, complement and coagulation cascades, COVID-19, and diabetic cardiomyopathy.

Complement factors are required for the anti-ALI effects of QFPD

The RNA-seq analysis and network pharmacology suggested that the complement-related pathway is important for the QFPD-mediated anti-inflammatory effect in ALI. The levels of complement components were measured in the serum and supernatant obtained from the cell culture by ELISA. The data revealed that after the LPS challenge, the production of C3a, C5a and C5b-9 significantly increased, while this induction was significantly re-

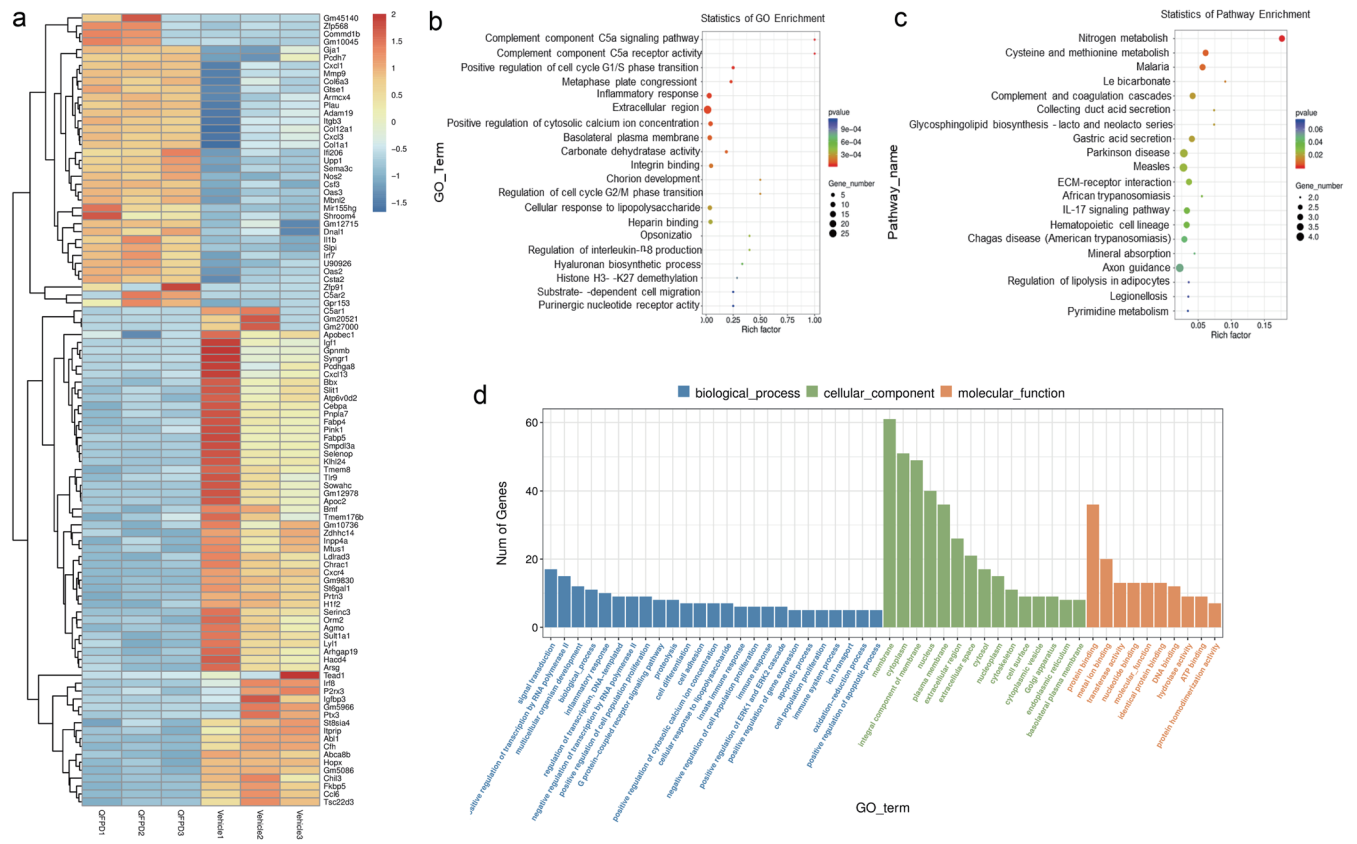


Fig. 4. Transcriptomics analysis of LPS-induced cell models after QFPD treatment. (a) Hierarchical clustering heat maps for the DEGs. (b and d) GO enrichment analysis of the DEGs of LPS+QFPD vs. LPS. (c) KEGG enrichment analysis for the DEGs of LPS+QFPD vs. LPS. DEGs, differentially expressed genes; GO, Gene Ontology; KEGG, Kyoto Encyclopaedia of Genes and Genomes; LPS, lipopolysaccharide; QFPD, Qingfei Paidu decoction.

duced after QFPD was simultaneously introduced (Fig. 7a and b). Furthermore, the expression level of C5aR in pulmonary cells was measured by IF assay through counterstaining with F4/80 to mark the macrophages. A similar inhibitory effect of QFPD on the C5aR expression was also observed (Fig. 7c and d).

In order to further ascertain that the therapeutic effect of QFPD on ALI is mediated by the complement pathway, siRNAs that target C3, C1s, CFD and MASP2, which are the key molecules of the complement pathway, classical pathway, bypass pathway, and lectin pathway, respectively (Polycarpou *et al.*, 2020),³⁴ were transfected to the macrophages. After LPS exposure, the silencing of the above complement factors restored the disturbance of apoptosis-associated proteins (Fig. 8a), and reduced the production of inflammatory factors (Fig. 8b–d). However, no obvious synergistic reduction in inflammatory factors and apoptosis was observed when the macrophages were treated by QFPD plus siRNA targeting C3 or C1s (Fig. 8a–d). Therefore, these results suggest that the classical pathway of complement factors is required for QFPD to achieve its therapeutic role in reducing inflammatory response and cytokine storm production, and protecting against ALI.

Discussion

The direct inhibition of the massive release of cytokines from hyperactivated immune cells serves as a therapeutic strategy for ALI

and SARS-CoV-2 infection.³⁵ To date, traditional Chinese medicine, including QFPD, has been widely used for the treatment of patients with COVID-19.³⁶ Compared to modern medicines, herb-based TCMs have exhibited several merits, including pronounced curative effects, fewer side effects, and lower costs.^{37,38} QFPD comprises of several Chinese herbal ingredients. Among these, licorice is one of the most important ingredients, and is a frequently used herb in Chinese formulas.³⁹ Furthermore, licorice, which is also known as the “National Venerable Master”,⁴⁰ has demonstrated its significant anti-inflammatory and antiviral effects that result from its components, such as gamma-linolenic acid, and its metabolite glycyrrhetic acid.⁴¹ Since acute lung injury is a common clinical symptom after COVID-19 infection, the effects of QFPD in ALI, and its potential mechanisms of activity were investigated through *in vivo* and *in vitro* experiments, and network pharmacology.

LPS is a bacterial endotoxin identified in gram-negative bacteria, and this serves as a classical inducer to construct inflammation models.⁴² LPS-induced CSS models were generated *in vitro*, and the results revealed that QFPD can inhibit TNF- α and IL6. In addition, the QFPD treatment reduced the inflammation in the lungs, as evidenced by the reduction in neutrophil infiltration and alveolar congestion. Furthermore, the total cell number in BALF significantly decreased after QFPD treatment, confirming the anti-inflammatory effect of QFPD. Therefore, QFPD holds a potential as an effective strategy for the treatment of ALI.

The core targets of QFPD in counteracting ALI were also

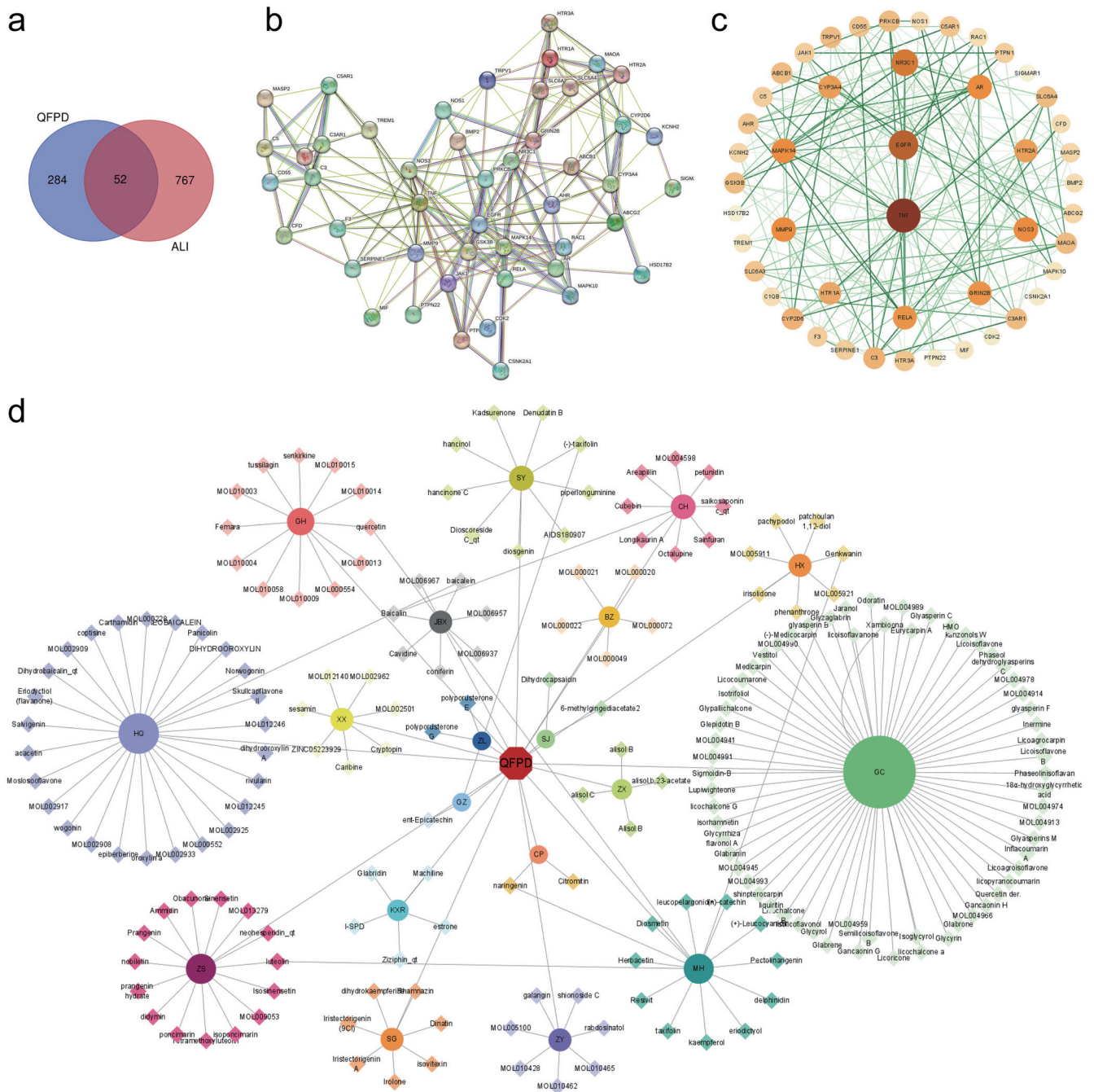


Fig. 5. Network pharmacology analysis for the targets of the QFPD treatment in ALI. (a) Venn diagram of potential targets of QFPD in the treatment. (b) PPI network diagram. (c) The TSV format file was downloaded from the STRING database, and imported to Cytoscape 3.9.1 for visual display. (d) The drug-herb-compound network. The red octagon represents the QFPD, the circles represent the herbs in QFPD, and the rhombuses represent the ingredients of each herb. ALI, acute lung injury; PPI, protein-protein interaction networks; QFPD, Qingfei Paidu decoction.

screened, and several factors, including TNF, EGFR, RELA and NR3C1, were predicted to be the core targets. The excessive production of TNF- α is closely correlated to the evolution of inflammatory illnesses, such as rheumatoid arthritis, inflammatory bowel disease, and acute respiratory distress syndrome (ARDS). Importantly, TNF- α is also crucial in the pathogenesis of COVID-19-associated cytokine storms, and the consequent progression

of disease severity.⁴ Epidermal growth factor receptor (EGFR) is a component of ALI, and serves as the key drug target in auto-inflammatory and auto-immune illnesses.⁴³ In addition, EGFR is associated with viral load, severity, criticality and prognosis in COVID-19 patients.⁴⁴ Furthermore, RELA and NR3C1 take part in inflammation and viral infections.^{45,46} Together, these potential targets of QFPD further support its value as an alternative treat-

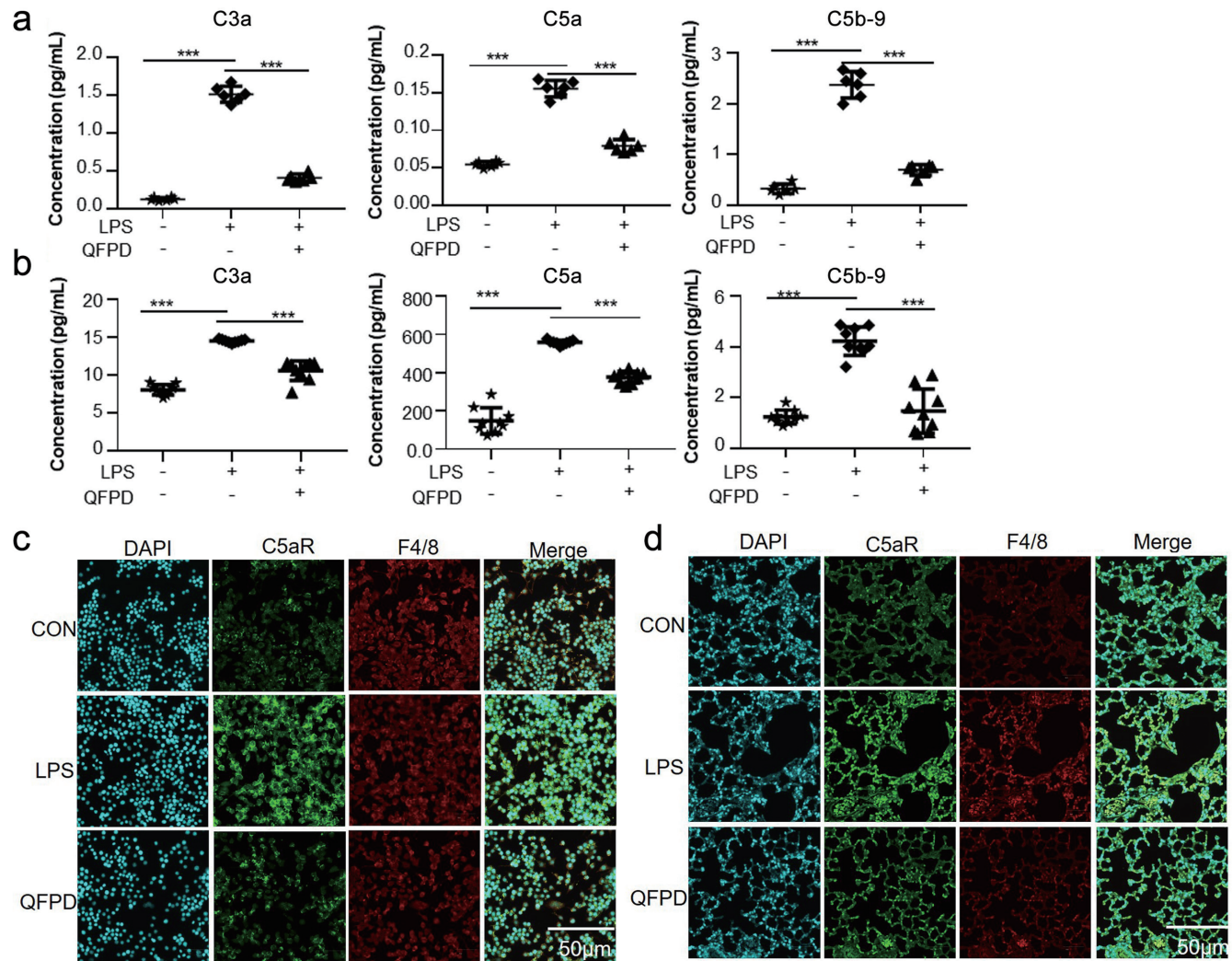


Fig. 7. The anti-inflammatory effects of QFPD were mediated through complement factors. QFPD inhibited C3a, C5a and C5b-9 *in vivo* (a) and *in vitro* (b). (c) Immunofluorescence staining of C5aR protein (magnification: 400 \times). (d) Tissue immunofluorescence staining of the C5aR and F4/80 protein (magnification: 400 \times). DAPI, 4',6-diamidino-2-phenylindole; LPS, lipopolysaccharide; QFPD, Qingfei Paidu decoction.

of QFPD in LPS-induced ALI through a suite of cell experiments and animal experiments. The network pharmacology and transcriptome analysis of the gene expression also demonstrated that QFPD inhibits ALI through the classical complement pathway. The next step is to investigate the disassembled prescriptions of traditional Chinese medicine compound prescriptions, and separate and track active ingredients with unique efficacy. The present study provides a practical basis and directional guide for the further exploration of the use of QFPD in treating ALI.

Conclusions

The present study explored the underlying mechanisms of the effects of QFPD on the treatment of ALI through network pharmacology, molecular docking, and experimental verification. The results indicated that the classical complement pathway is the main target for QFPD in ALI treatment. These results provide a practical basis and directional guide for further exploration of the use of QFPD in treating ALI.

Supporting information

Supplementary material for this article is available at <https://doi.org/10.14218/ERHM.2022.00127>.

Supplementary Table 1. Design of the potential small interfering RNA sequences.

Supplementary Table 2. Analysis of blood test in LPS-induced CSS mice. Data are expressed as mean \pm standard deviation (SD, $n = 9$), * $p < 0.05$, ** $p < 0.01$, *** $p < 0.001$; Lymph#, lymphocytes; Mon#, monocytes; Gran#, granulocytes; CSS, cytokine storm syndrome; LPS, lipopolysaccharide; ns, no significance; WBC, white blood cells.

Supplementary Table 3. Drug-ingredients list.

Supplementary Fig. 1. (a) Fingerprint of the Qingfei Paidu Decoction; (b) mixed references solution of the seven components: 1-chlorogenic acid; 2-amygdalin; 3-geniposide; 4-liquiritin; 5-hesperidin;

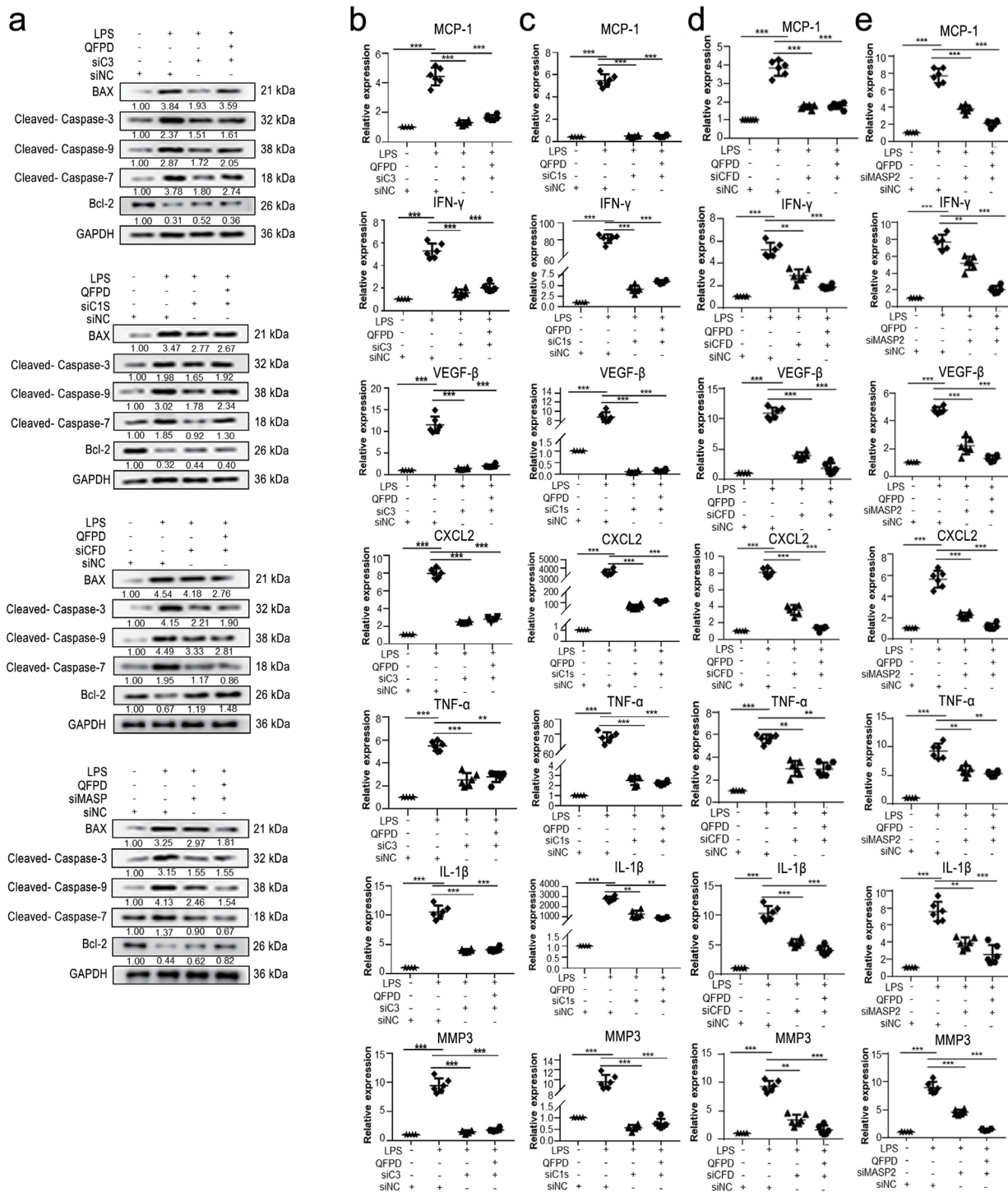


Fig. 8. The silencing of complement factors abolished the protective effect of QFPD on LPS-induced CSS. (a) Macrophages with or without C3, C1s, CFDP and MASP2 silencing were treated with QFPD or vehicle for 24 hours, and the protein expression of Bax, caspase-3, cleaved-caspase-9, cleaved-caspase-7 and Bcl-2 were measured by western blot to detect the apoptosis in macrophages. (b–e) After exposure to LPS for six hours, macrophages with or without C3, C1s, CFDP and MASP2 silencing were treated with QFPD or vehicle for an additional 24 hours. The MCP-1, IFN- γ , VEGF- β , CXCL2, TNF- α , IL1 β and MMP3 levels in the macrophage supernatants were analyzed by qRT-PCR. The data presents the six samples, which were obtained from one representative experiment of three independent experiments with similar results. The statistical analysis was performed using one-way ANOVA, followed by Tukey-Kramer post-test, ** $p < 0.01$, *** $p < 0.001$, compared to the control group. ANOVA, one-way analysis of variance; CSS, cytokine storm syndrome; CXCL2, C-X-C Motif Chemokine Ligand 2; IFN- γ , interferon-gamma; LPS, lipopolysaccharide; MCP-1, monocyte chemoattractant protein-1; MMP3, matrix metalloproteinase 3; TNF- α , tumor necrosis factor-alpha; QFPD, Qingfei Paidu decoction, VEGF- β , vascular endothelial growth factor- β .

6-baicalin; 7-ammonium glycyrrhizinate; 8-saikosaponins.

Supplementary Fig. 2. Molecular docking diagram for the compound and target.

Acknowledgments

We would like to thank the members in the laboratory for their assistance and support.

Funding

This work was supported by the National Natural Science Foundation of China (Grant nos. 81772760, 82072850, 81901666, 82101903 and 82171801), the Shandong Taishan Scholarship (Grant no. tsqn20161076), the Natural Science Foundation of Shandong Province (Grant no. ZR2020YQ55), the Key Research and Development Project of Shandong Province (No. 2021ZDSYS27), the Innovation Project of Shandong Academy of Medical Sciences (2021), the Youth Innovation Technology Plan of Shandong University (Grant no. 2019KJK003), and the Academic Promotion Programme of Shandong First Medical University (Grant no. 2019LJ001).

Conflict of interest

The authors have no conflict of interests to disclose.

Author contributions

DDS: methodology, investigation, and writing of the original draft; LNG: investigation and writing of the original draft; LY: animal experiments; YZ and TW: validation; YG and HCF: quality control of the QFPD; RJZ: formal analysis; ZRS and LJH: validation; JLZ: visualization; SFL and YL: software; HJS: QFPD preparation; JHP: data curation; GHS: supervision and writing (review and editing); LW: supervision, methodology, and writing (review and editing).

Ethical statement

All animal studies were approved by the Institutional Animal Care and Use Committee of Shandong First Medical University & Shandong Academy of Medical Sciences (SMBC21LL028).

Data sharing statement

No additional data are available.

References

- [1] Mokrá D. Acute lung injury - from pathophysiology to treatment. *Physiol Res* 2020;69(Suppl 3):S353–S366. doi:10.33549/physiolres.934602, PMID:33464919.
- [2] Liu Y, Xiang D, Zhang H, Yao H, Wang Y. Hypoxia-inducible factor-1: A potential target to treat acute lung injury. *Oxid Med Cell Longev* 2020;2020:8871476. doi:10.1155/2020/8871476, PMID:33282113.
- [3] Yang B, Ma L, Wei Y, Cui Y, Li X, Wei Y, *et al.* Isorhamnetin alleviates lipopolysaccharide-induced acute lung injury by inhibiting mTOR signaling pathway. *Immunopharmacol Immunotoxicol* 2022;44(3):387–399. doi:10.1080/08923973.2022.2052892, PMID:35306954.
- [4] Karki R, Sharma BR, Tuladhar S, Williams EP, Zalduondo L, Samir P, *et al.* Synergism of TNF- α and IFN- γ triggers inflammatory cell death, tissue damage, and mortality in SARS-CoV-2 infection and cytokine shock syndromes. *Cell* 2021;184(1):149–168.e17. doi:10.1016/j.cell.2020.11.025, PMID:33278357.
- [5] Al-Kuraishy HM, Al-Gareeb AI, Al-Hussaniy HA, Al-Harcana NAH, Alexiou A, Batiha GE. Neutrophil Extracellular Traps (NETs) and Covid-19: A new frontiers for therapeutic modality. *Int Immunopharmacol* 2022;104:108516. doi:10.1016/j.intimp.2021.108516, PMID:35032828.
- [6] Ahmed-Hassan H, Sisson B, Shukla RK, Wijewantha Y, Funderburg NT, Li Z, *et al.* Innate immune responses to highly pathogenic coronaviruses and other significant respiratory viral infections. *Front Immunol* 2020;11:1979. doi:10.3389/fimmu.2020.01979, PMID:32973803.
- [7] Butt Y, Kurdowska A, Allen TC. Acute lung injury: A clinical and molecular review. *Arch Pathol Lab Med* 2016;140(4):345–350. doi:10.5858/arpa.2015-0519-RA, PMID:27028393.
- [8] Mokra D, Kosutova P. Biomarkers in acute lung injury. *Respir Physiol Neurobiol* 2015;209:52–58. doi:10.1016/j.resp.2014.10.006, PMID:25466727.
- [9] Racanelli AC, Kikers SA, Choi AMK, Cloonan SM. Autophagy and inflammation in chronic respiratory disease. *Autophagy* 2018;14(2):221–232. doi:10.1080/15548627.2017.1389823, PMID:29130366.
- [10] Hou F, Xiao K, Tang L, Xie L. Diversity of macrophages in lung homeostasis and diseases. *Front Immunol* 2021;12:753940. doi:10.3389/fimmu.2021.753940, PMID:34630433.
- [11] Hung CM, Peng CK, Yang SS, Shui HA, Huang KL. WNK4-SPAK modulates lipopolysaccharide-induced macrophage activation. *Biochem Pharmacol* 2020;171:113738. doi:10.1016/j.bcp.2019.113738, PMID:31786261.
- [12] Broug-Holub E, Toews GB, van Iwaarden JF, Strieter RM, Kunkel SL, Paine R 3rd, *et al.* Alveolar macrophages are required for protective pulmonary defenses in murine Klebsiella pneumonia: elimination of alveolar macrophages increases neutrophil recruitment but decreases bacterial clearance and survival. *Infect Immun* 1997;65(4):1139–1146. doi:10.1128/iai.65.4.1139-1146.1997, PMID:9119443.
- [13] Chen J, Wang YK, Gao Y, Hu LS, Yang JW, Wang JR, *et al.* Protection against COVID-19 injury by qingfei paidu decoction via anti-viral, anti-inflammatory activity and metabolic programming. *Biomed Pharmacother* 2020;129:110281. doi:10.1016/j.biopha.2020.110281, PMID:3255425.
- [14] Wu Y, Xu L, Cao G, Min L, Dong T. Effect and mechanism of Qingfei Paidu decoction in the management of pulmonary fibrosis and COVID-19. *Am J Chin Med* 2022;50(1):33–51. doi:10.1142/S0192415X22500021, PMID:34931591.
- [15] Yang Y, Islam MS, Wang J, Li Y, Chen X. Traditional Chinese Medicine in the treatment of patients infected with 2019-new coronavirus (SARS-CoV-2): A review and perspective. *Int J Biol Sci* 2020;16(10):1708–1717. doi:10.7150/ijbs.45538, PMID:32226288.
- [16] Afshar-Kharghan V. The role of the complement system in cancer. *J Clin Invest* 2017;127(3):780–789. doi:10.1172/JCI90962, PMID:28248200.
- [17] Mastellos D, Germenis AE, Lambris JD. Complement: an inflammatory pathway fulfilling multiple roles at the interface of innate immunity and development. *Curr Drug Targets Inflamm Allergy* 2005;4(1):125–127. doi:10.2174/1568010053622993, PMID:15720246.
- [18] Triantafilou M, Hughes TR, Morgan BP, Triantafilou K. Complementing the inflammasome. *Immunology* 2016;147(2):152–164. doi:10.1111/imm.12556, PMID:26572245.
- [19] Chauhan AJ, Wiffen LJ, Brown TP. COVID-19: A collision of complement, coagulation and inflammatory pathways. *J Thromb Haemost* 2020;18(9):2110–2117. doi:10.1111/jth.14981, PMID:32608159.
- [20] Guo RF, Ward PA. Role of C5a in inflammatory responses. *Annu Rev Immunol* 2005;23:821–852. doi:10.1146/annurev.immunol.23.021704.115835, PMID:15771587.
- [21] Pineda-Torra I, Gage M, de Juan A, Pello OM. Isolation, culture, and polarization of murine bone marrow-derived and peritoneal macrophages. *Methods Mol Biol* 2015;1339:101–109. doi:10.1007/978-1-4939-2929-0_6, PMID:26445783.
- [22] Guo B, Zhao C, Zhang C, Xiao Y, Yan G, Liu L, *et al.* Elucidation of the anti-inflammatory mechanism of Er Miao San by integrative approach of network pharmacology and experimental verification. *Pharmacol Res* 2022;175:106000. doi:10.1016/j.phrs.2021.106000, PMID:34838694.
- [23] Li X, Wei S, Niu S, Ma X, Li H, Jing M, *et al.* Network pharmacology prediction and molecular docking-based strategy to explore

- the potential mechanism of Huanglian Jiedu Decoction against sepsis. *Comput Biol Med* 2022;144:105389. doi:10.1016/j.compbiomed.2022.105389, PMID:35303581.
- [24] Li Z, Liu Q, Zhu Y, Wu L, Liu W, Li J, *et al*. Network pharmacology, molecular docking, and experimental validation to unveil the molecular targets and mechanisms of compound fuling granule to treat ovarian cancer. *Oxid Med Cell Longev* 2022;2022:2896049. doi:10.1155/2022/2896049, PMID:36062197.
- [25] Li X, Ma J, Guo L, Dong C, Zhu G, Hong W, *et al*. Identification of bioactive compounds and potential mechanisms of kuntai capsule in the treatment of polycystic ovary syndrome by integrating network pharmacology and bioinformatics. *Oxid Med Cell Longev* 2022;2022:3145938. doi:10.1155/2022/3145938, PMID:35528524.
- [26] Wang CR, Chen HW, Li Y, Zhou MY, Wong VK, Jiang ZH, *et al*. Network pharmacology exploration reveals anti-apoptosis as a common therapeutic mechanism for non-alcoholic fatty liver disease treated with blueberry leaf polyphenols. *Nutrients* 2021;13(11):4060. doi:10.3390/nu13114060, PMID:34836315.
- [27] Wang X, Shen Y, Wang S, Li S, Zhang W, Liu X, *et al*. PharmMapper 2017 update: a web server for potential drug target identification with a comprehensive target pharmacophore database. *Nucleic Acids Res* 2017;45(W1):W356–W360. doi:10.1093/nar/gkx374, PMID:28472422.
- [28] Yao ZJ, Dong J, Che YJ, Zhu MF, Wen M, Wang NN, *et al*. TargetNet: A web service for predicting potential drug-target interaction profiling via multi-target SAR models. *J Comput Aided Mol Des* 2016;30(5):413–424. doi:10.1007/s10822-016-9915-2, PMID:27167132.
- [29] Li H, You J, Yang X, Wei Y, Zheng L, Zhao Y, *et al*. Glycyrrhetic acid: A potential drug for the treatment of COVID-19 cytokine storm. *Phytomedicine* 2022;102:154153. doi:10.1016/j.phymed.2022.154153, PMID:35636166.
- [30] Ruan X, Du P, Zhao K, Huang J, Xia H, Dai D, *et al*. Mechanism of Dayuanyin in the treatment of coronavirus disease 2019 based on network pharmacology and molecular docking. *Chin Med* 2020;15:62. doi:10.1186/s13020-020-00346-6, PMID:32536965.
- [31] Kong Q, Wu Y, Gu Y, Lv Q, Qi F, Gong S, *et al*. Analysis of the molecular mechanism of Pudinilone (PDL) treatment for COVID-19 by network pharmacology tools. *Biomed Pharmacother* 2020;128:110316. doi:10.1016/j.biopha.2020.110316, PMID:32505821.
- [32] Yuan Y, Zhang Y, Zheng R, Yuan H, Zhou R, Jia S, *et al*. Elucidating the anti-aging mechanism of Si Jun Zi Tang by integrating network pharmacology and experimental validation in vivo. *Aging (Albany NY)* 2022;14(9):3941–3955. doi:10.18632/aging.204055, PMID:35537009.
- [33] Yang R, Liu H, Bai C, Wang Y, Zhang X, Guo R, *et al*. Chemical composition and pharmacological mechanism of Qingfei Paidu Decoction and Ma Xing Shi Gan Decoction against Coronavirus Disease 2019 (COVID-19): In silico and experimental study. *Pharmacol Res* 2020;157:104820. doi:10.1016/j.phrs.2020.104820, PMID:32360484.
- [34] Polycarpou A, Howard M, Farrar CA, Greenlaw R, Fanelli G, Wallis R, *et al*. Rationale for targeting complement in COVID-19. *EMBO Mol Med* 2020;12(8):e12642. doi:10.15252/emmm.202012642, PMID:32559343.
- [35] Shawki MA, Elsayed NS, Mantawy EM, Said RS. Promising drug repurposing approach targeted for cytokine storm implicated in SARS-CoV-2 complications. *Immunopharmacol Immunotoxicol* 2021;43(4):395–409. doi:10.1080/08923973.2021.1931302, PMID:34057871.
- [36] Ge L, Zhu H, Wang Q, Li M, Cai J, Chen Y, *et al*. Integrating Chinese and western medicine for COVID-19: A living evidence-based guideline (version 1). *J Evid Based Med* 2021;14(4):313–332. doi:10.1111/jebm.12444, PMID:34632732.
- [37] Wang J, Qi F. Traditional Chinese medicine to treat COVID-19: the importance of evidence-based research. *Drug Discov Ther* 2020;14(3):149–150. doi:10.5582/ddt.2020.03054, PMID:32669523.
- [38] Tong T, Wu YQ, Ni WJ, Shen AZ, Liu S. The potential insights of Traditional Chinese Medicine on treatment of COVID-19. *Chin Med* 2020;15:51. doi:10.1186/s13020-020-00326-w, PMID:32483409.
- [39] Sun J, Zhang Q, Yang G, Li Y, Fu Y, Zheng Y, *et al*. The licorice flavonoid isoliquiritigenin attenuates Mycobacterium tuberculosis-induced inflammation through Notch1/NF- κ B and MAPK signaling pathways. *J Ethnopharmacol* 2022;294:115368. doi:10.1016/j.jep.2022.115368, PMID:35589023.
- [40] Guo J, Shang E, Zhao J, Fan X, Duan J, Qian D, *et al*. Data mining and frequency analysis for licorice as a “Two-Face” herb in Chinese Formulae based on Chinese Formulae Database. *Phytomedicine* 2014;21(11):1281–1286. doi:10.1016/j.phymed.2014.07.006, PMID:25172790.
- [41] Leite CDS, Bonafé GA, Carvalho Santos J, Martinez CAR, Ortega MM, Ribeiro ML. The Anti-Inflammatory Properties of Licorice (Glycyrrhiza glabra)-Derived Compounds in Intestinal Disorders. *Int J Mol Sci* 2022;23(8):4121. doi:10.3390/ijms23084121, PMID:35456938.
- [42] Luo W, Yang LB, Qian CC, Ma B, Manjengwa GM, Miao XM, *et al*. Flavokawain B alleviates LPS-induced acute lung injury via targeting myeloid differentiation factor 2. *Acta Pharmacol Sin* 2022;43(7):1758–1768. doi:10.1038/s41401-021-00792-4, PMID:34737421.
- [43] Mindur JE, Swirski FK. Growth Factors as Immunotherapeutic Targets in Cardiovascular Disease. *Arterioscler Thromb Vasc Biol* 2019;39(7):1275–1287. doi:10.1161/ATVBAHA.119.311994, PMID:31092009.
- [44] Abdo Cuza AA, Ávila JP, Martínez RM, González JJ, Aspuro GP, Gutiérrez Martínez JA, *et al*. Nimotuzumab for COVID-19: case series. *Immunotherapy* 2022;14(3):185–193. doi:10.2217/imt-2021-0269, PMID:34806405.
- [45] Newton R. Anti-inflammatory glucocorticoids: changing concepts. *Eur J Pharmacol* 2014;724:231–236. doi:10.1016/j.ejphar.2013.05.035, PMID:23747654.
- [46] Brasier AR, Tian B, Jamaluddin M, Kalita MK, Garofalo RP, Lu M. RelA Ser276 phosphorylation-coupled Lys310 acetylation controls transcriptional elongation of inflammatory cytokines in respiratory syncytial virus infection. *J Virol* 2011;85(22):11752–11769. doi:10.1128/JVI.05360-11, PMID:21900162.
- [47] Polidoro RB, Hagan RS, de Santis Santiago R, Schmidt NW. Overview: Systemic Inflammatory Response Derived From Lung Injury Caused by SARS-CoV-2 Infection Explains Severe Outcomes in COVID-19. *Front Immunol* 2020;11:1626. doi:10.3389/fimmu.2020.01626, PMID:32714336.
- [48] Cabler SS, French AR, Orvedahl A. A Cytokine Circus with a Viral Ringleader: SARS-CoV-2-Associated Cytokine Storm Syndromes. *Trends Mol Med* 2020;26(12):1078–1085. doi:10.1016/j.molmed.2020.09.012, PMID:33051104.
- [49] Kim DM, Kim Y, Seo JW, Lee J, Park U, Ha NY, *et al*. Enhanced eosinophil-mediated inflammation associated with antibody and complement-dependent pneumonic insults in critical COVID-19. *Cell Rep* 2021;37(1):109798. doi:10.1016/j.celrep.2021.109798, PMID:34587481.
- [50] Chouaki Benmansour N, Carvelli J, Vivier É. [Involvement of the complement cascade in severe forms of COVID-19]. *Med Sci (Paris)* 2021;37(4):333–341. doi:10.1051/medsci/2021021, PMID:33835019.
- [51] Alosaimi B, Mubarak A, Hamed ME, Almutairi AZ, Alrashed AA, AlJuryyan A, *et al*. Complement anaphylatoxins and inflammatory cytokines as prognostic markers for COVID-19 severity and in-hospital mortality. *Front Immunol* 2021;12:668725. doi:10.3389/fimmu.2021.668725, PMID:34276659.
- [52] Chouaki Benmansour N, Carvelli J, Vivier E. Complement cascade in severe forms of COVID-19: Recent advances in therapy. *Eur J Immunol* 2021;51(7):1652–1659. doi:10.1002/eji.202048959, PMID:33738806.
- [53] Mummid S, Das NA, Carpenter AJ, Yoshida T, Yariswamy M, Mostany R, *et al*. RECK suppresses interleukin-17/TRAFF3IP2-mediated MMP-13 activation and human aortic smooth muscle cell migration and proliferation. *J Cell Physiol* 2019;234(12):22242–22259. doi:10.1002/jcp.28792, PMID:31074012.